The Structure of Thermal Plumes and Geophysical Observations

Scott D. King and Hannah L. Redmond

Dept. of Earth and Atmospheric Sciences

Purdue University, West Lafayette, Indiana

ABSTRACT

We present a sequence of numerical experiments studying thermal plumes that arise from the basal thermal boundary layer in a spherical axisymmetric convecting fluid, reporting the geoid, topographic (swell), and heatflow anomalies. We consider the influence of spherical geometry, temperature-and pressure-dependence of rheology, internal heat generation, pressure-dependent coefficient of thermal expansion, the Clapeyron slope of the endothermic phase transformation, and compositional layering at the base of the mantle on the structure and dynamics of thermal plumes and resulting geophysical anomalies. This fluid system simplifies a number of complexities within the Earth (e.g., it is not compressible, does not include plate motions, enforces axisymmetric symmetry, and has a simple equation of state); however, this system is computationally tractable and provides an opportunity to evaluate each effect in a systematic fashion. With the assumptions listed above we are formally unable to reproduce the observed hotspot swell, heatflow, and geoid anomalies from the resulting thermal plumes. The calculations that most closely approach the observed geoid, topographic and heatflow anomalies contain all the effects mentioned above. One particularly interesting aspect of these calculations is that when we include depth-dependent coefficient of thermal expansion the plume conduits in the lower 500 kilometers of the mantle are more than 200 km in diameter wider than with an otherwise identical, uniform coefficient of thermal expansion calculation. We speculate that the lack of mobile plates in our calculations, which would both advect upwelling material away from the plume conduit and change the global cooling mechanism, is a major shortcoming and that it may be possible to reconcile thermal plume calculations with the geoid, topography, and heatflow observations if we included mobile plates.

INTRODUCTION

Thermal plumes, originating at the core mantle boundary have become the standard explanation for hotspot volcanism (e.g., Morgan, 1971; Burke and Wilson, 1976; Davies, 1988; Sleep, 1990; Griffiths and Campbell, 1990; 1991; Hill et al., 1992; Davies and Richards, 1992; Schubert et al., 2001). The plume hypothesis has benefited from elegant fluid dynamical theory and tank models (e.g., Whitehead and Luther, 1975; Olson and Singer, 1985; Griffiths, 1986; Griffiths and Campbell, 1990; 1991; Davaille, 1999; Davaille and Vatterville, 2005). However the primary geophysical observations of heatflow, geoid, and topographic swell anomalies are difficult to reproduce in laboratory experiments, as are the effects of pressure-dependent material properties. Calculations of thermal plumes have focused on temperature-dependent rheology, phase transformations, and equation of state (e.g., Kiefer and Hager, 1992; Sleep, 1992; Kellogg and King, 1993; Sleep, 1994; Farnetani and Richards, 1994; 1995; Schubert et al., 1995; Davies, 1995; Ratcliff et al., 1996; Sleep, 1996; Farnetani et al., 1996; van Keken, 1997; Kellogg and King, 1997; King, 1997; Farnetani, 1997; Goes et al., 2004; Farnetani and Samuel, 2005; Lin and van Keken, 2006a; 2006b; Zhong, 2006). Given improvements in our understanding of the properties of the mantle in the last decade, it is useful to reassess how phase transformations, rheology, equation of state, and composition influence the structure, vigor and other observable properties of plumes in the mantle. The hypothesis tested here is that by including these effects, we can produce geoid, topography, and heatflow anomalies that are consistent with the observed hotspot anomalies. While the influence of these parameters has been studied in general convection calculations, less attention has been paid to mantle plumes and the resulting geophysical anomalies. Here we build systematically, varying one parameter at a time, and focus specifically on comparing the anomalies produced by thermal plumes with observations at

hotspots. This work builds on previous work by a variety of investigators, including Kiefer and Hager (1992), Schubert et al. (1995), Davies (1995), King (1997), and Goes et al. (2004). We do not discuss the effect of chemical layering in the mid-mantle or a fully self-consistent equation of state (c.f., Ita and King, 1994), both of which should be investigated in future studies.

The first question is why instabilities from the core-mantle boundary should be expected. This can be addressed in a number of different ways, and while the following remarks are not meant to be exhaustive, they provide the reader with a flavor of the arguments and further references. First, thermal boundary layer instabilities, usually referred to as plumes in the fluid dynamical literature, are a natural consequence of the cooling of the Earth (c.f., Schubert, 1979; Davies, 1980). It is generally accepted that Earth was strongly heated during formation (c.f., Safranov, 1978; Wetherill, 1990). This initially hot mantle cools, largely by plate-scale mantle flow and cooling of the surface boundary layer (c.f., Davies, 1988). As the mantle cools, the temperature difference between the mantle and core grows and a thermal boundary layer between the mantle and core forms (e.g., Stacey and Loper, 1983). As this thermal boundary layer grows, it reaches a point where it becomes gravitationally unstable and instabilities form at this thermal boundary layer (c.f., Stacey and Loper, 1983; Olson et al., 1987; Sleep et al., 1988). Further details can be found in (Stacey and Loper, 1983; Schubert et al., 2001). These instabilities take the form of cylindrical plume-like upwellings where the morphology depends on the rheology (e.g., Kellogg and King, 1997). All of these studies rely on fairly simple fluid approximations of the mantle (i.e., incompressible, chemically homogeneous, constant coefficient of thermal expansion). Estimates of the temperature contrast across the core mantle boundary can be made by extrapolating the melting temperature of iron from the inner core boundary through the outer core and extrapolating the geotherm through the mantle to the core-

mantle boundary (e.g., Anderson, 2002), leading to an estimate of a 1000-1800 degree temperature change between the mantle and the core. This temperature difference is presumably concentrated at the base of the mantle (e.g., Anderson, 2002; Buffett, 2003). This is a large temperature difference (with a fairly large uncertainty) and it is not only a problem for the thermal evolution of the core and Earth's magnetic field (Buffett, 2003), it is a problem for the mantle plume hypothesis, because the geochemistry and petrology of hotspot lavas require a fairly small potential temperature increase of at most several hundred degrees at the melting source (e.g., Farnetani, 1997) and small heat flow anomaly (e.g,. DeLaughter et al., 2005). Recent calculations that show that the lower mantle may be subadiabatic with a superadiabatic region above the core-mantle boundary (e.g., Bunge et al., 2001; Monnereau and Yuen, 2002; Zhong, 2006); this reduces the problem to some extent. This problem will be examined further in the discussion.

There is an alternative to the thermal plume hypothesis. Nakagawa and Tackley (2004) show that a thermochemical model of the lower mantle could develop broad superplumes consistent with the long wavelength seismic structure and the thermal evolution develops isolated reservoirs that would be consistent with the geochemical observations. Monnereau and Yuen (2002) show similar broad, sluggish features in compressible spherical convection calculations with depth-dependent rheology and depth-dependent coefficient of thermal expansion. Schubert et al. (2004) suggest that the seismic data are consistent with a spatial cluster of smaller plumes.

The second line of reasoning for the inevitability of plumes comes from scaling analysis. The Rayleigh number of a fluid governs the convective vigor of the fluid (c.f., Chandrasekhar,

1961). One can think of the Rayleigh number as the ratio of the two forces that are balanced in viscous flow: buoyancy and viscous drag. The Rayleigh number takes the form

$$Ra = \frac{\rho g \alpha \Delta T D^3}{\kappa \eta} \quad (1)$$

where ρ is the average mantle density, g is the acceleration due to gravity, α is the coefficient of thermal expansion, ΔT is the temperature-drop across the fluid, D is the depth of the fluid, κ is the thermal diffusivity, and η is the viscosity. Typical ranges of the values of these parameters (and references) are given in Table 1. The Rayleigh number does not reflect the changes of the properties of the fluid with pressure or temperature, hence as one studies more complex fluid systems, the Rayleigh number becomes a limited diagnostic and one must be careful to define how the variable properties are used in the definition of the Rayleigh number. For example, in thermo-chemical systems, a second 'chemical' Rayleigh number can be introduced (e.g., Farnetani and Richards, 1995) and the dynamics of the fluid can be mapped out with these two parameters. A limitation of Rayleigh number scaling is that it can not predict the interaction or feedback between parameters. For example, consider a fluid with a substantial source of heat below that is only cooling by conduction. Conduction is a less efficient means of heat transport than convection, and if the rate of heat being supplied from below exceeds the rate at which heat can be conducted through the fluid, the fluid temperature will rise. If, like the mantle, the fluid has a rheology that is a strong function of temperature, as the temperature rises, the viscosity decreases and the fluid will eventually become convectively unstable. It is increasingly apparent that there are non-linear interactions between the depth-variable and temperature variable properties that are not well understood at this time (c.f., Dubuffett and Yuen, 2000; Matyska and Yuen, 2005).

Third, both stability analysis and numerical models of mantle convection show that 3D quasi-cylindrical upwellings (i.e., plumes) are the dominant planform of convection in spherical geometry (c.f., Busse, 1975; Zebib et al., 1980; Busse and Riahi, 1982; Zebib et al., 1985; Bercovici et al., 1989; Tackley et al., 1993; 1994; Ratcliff et al., 1995; Zhang and Yuen, 1995; Bunge et al., 1996; 1997; Farnetani et al., 2005; Zhong, 2006). In all calculations presented, plume-like upwellings are observed although most of these use a Bousinessq approximation and a no chemical layering.

It is worth noting, that there is a potentially viable alternative model where the properties of the lower mantle lead to thermal instabilities at the base of the mantle that are long-wavelength, large-scale, 'superplumes' (c.f., Wen and Anderson, 1997a 1997b; Davaille, 1999; Nakagawa and Tackley, 2004; Anderson, 2005a; 2005b) that may form over a timescale of hundreds of millions of years (or longer). Within the framework of this hypothesis, hotspots would be caused by local compositional anomalies (c.f., Anderson, 2005a), instabilities within the upper mantle from deep superplumes (Courtillot et al., 2003), or lithsopheric effects (King and Ritsema, 2000). Courtillot et al. (2003) and Davaille (1999) suggest that this mode of convection could operate in conjunction with a deep, narrow plume mode. We will not be investigating this hypothesis in this study.

Geophysical observations related to hotspots include the geoid, topographic, and heatflow anomalies; in addition to the hotspot track itself (e.g., Crough and Jurdy, 1980; Crough, 1983; Davies, 1988; Sleep, 1990; Goes et al., 2004; Anderson and Schramm, 2005; Sandwell et al., 2005; Anderson, 2005a; DeLaughter et al., 2005; Zhong, 2006). There are also important geochemical observations from hotspot lavas that provide insight into composition, temperature, and melting history of hotspot lavas and these have been investigated in a number of numerical

studies (e.g., Ribe and Christensen, 1994a; Farnetani and Richards, 1995; Farnetani et al., 1996; Samuel and Farnetani, 2003). We will not consider melting here, although clearly one of the most critical aspects of hotspots is the associated volcanic activity. Calculations with an endothermic phase transformation and internal heating show that the majority of the lower mantle may be subadiabatic with a superadiabatic temperature gradient near the core mantle boundary (e.g., Bunge et al., 2001; Monnereau and Yuen, 2002; Zhong, 2006). As much as 300-500 degrees of the temperature-difference across the core may be explained by subadiabicity of the lower mantle.

Seismologists have imaged velocity anomalies beneath hotspot regions (Nataf and van Decar, 1993; Wolfe et al., 1997; Wolfe, 1998; Bijwaard and Spakman, 1999; Foulger et al., 2000; Humphreys et al., 2000; Allen et al., 2002; Ritsema and Allen, 2003; Montelli et al., 2003). There is a tradeoff between the magnitude of a seismic anomaly and the width of the anomaly in seismic imaging (e.g., Allen and Tromp, 2005) and there is limited resolution with depth below 400 km depth in studies that specifically attempt to image anomalies below hotspots, due to the restricted geometry of the stations and receivers (Wolfe et al., 1997; Wolfe, 1998; Foulger et al., 2000; Humphreys et al., 2000; Allen et al., 2002).

The specific observations that we will use to constrain the plume calculations are the heatflow, geoid, and topographic anomalies and to a lesser extent the width of the seismic anomaly beneath hotspots, which we take from seismic tomography (e.g., Wolfe, 1998; Foulger et al., 2000; Humphreys et al., 2000; Allen et al., 2002; Allen and Tromp, 2005). As will become apparent, exact values of the geophysical observations are not critical for this exercise, because many of our plume calculations create anomalies that are an order of magnitude larger than the hotspot observations. Given the uncertainties currently associated with many of the

parameters, we do not see much value in attempting to vary the model parameters until we achieve specific values of the hotspot observations. The goal here is to evaluate and illustrate the importance of the effects,

Heatflow anomalies at hotspot swells are small. Davies (1988) estimates that plume flow makes up less than 10% of the total heatflow of the surface of the Earth while DeLaughter et al., (2005) suggest that it is significantly less than this. Sleep estimates that the total contribution to the global surface heatflow of the Earth from approximately 40 plumes is 4 mW/m^2 (Sleep, 1990). Heatflow measurements are sparse, even for some of the best-studied hotspots; however heatflow observations from Hawaii suggest that the peak anomaly is less than 10-20 mW/m^2 (Von Hertzen et al., 1989) and probably is significantly less than this (DeLaughter et al., 2005). The possibility that heat is redistributed by hydrothermal circulation in the crust (Harris et al., 2000) cannot be ruled out and further complicates the interpretation of the heatflow observations. We will consider a peak heatflow anomaly less than 10 mW/m^2 as consistent with the observations, although we note that for many hotspots, this may be a generous estimate.

The geoid anomaly associated with hotspot swells is on the order of a few meters to at most 10 meters (e.g., Sleep, 1990). While there are significantly better geoid models available now with the GRACE data, the results presented by Sleep do not change significantly. Therefore, we consider peak geoid anomalies less than 10 meters as consistent with the observations. With both the geoid and topographic anomalies it is important to remember that the plume calculations here do not include the volcanic construction or underplating of magma beneath the lithosphere, which could be a significant part of the shorter wavelength anomaly. When looking at the geoid and topographic swell data, we are looking at longer wavelength (i.e.,

1,000-2,000 km) anomalies that most likely reflect the dynamic contribution to the geoid and topography rather than crustal or lithospheric structure (c.f., Richards et al., 1988; Sleep, 1990).

Topographic swell anomalies estimated for 26 hotspots range from 500-2500 meters with most swells in the 500-1200 meter range and the largest swell over Ethiopia (Crough, 1983). Hotspots occur on ridges, young and old oceanic lithosphere and beneath continents. There is no clear correlation between the magnitude of the hotspot swell and the lithosphere type or thickness, which again suggests that the swell is reflecting deeper mantle dynamics and not crustal or lithospheric structure. We consider peak topographic swells of less than 2000 meters as consistent with the hotspot observations, although we note that there are many hotspot swells significantly smaller than this.

While there is some ambiguity in the imaged seismic structures in the upper mantle beneath hotspots, and there is a tradeoff between the width and the magnitude of the anomalies, a 200-km wide anomaly in the upper mantle appears to be consistent with the seismic observations (Goes et al., 2004). While seismic studies image a low velocity anomaly in the upper mantle that may be as narrow as 100 km (e.g., Foulger et al., 2000; Allen et al., 2002) our calculations will have plume material ponding beneath the lithosphere because there is no plate flow advecting this material away from the plume tail in our calculations. Thus we are cautious about interpreting the detailed upper mantle structure in these calculations. We also point out that Goes et al. (2004) show that when converting temperature structures from thermal plume calculations to seismic velocity anomalies, that the resulting seismic velocity anomalies are significantly broader than the thermal anomalies.

While there have been a number of previous calculations that have investigated the effect of rheology (e.g., van Keken, 1997; Kellogg and King, 1997; Goes et al., 2004; Schott and Yuen,

2004) and phase transformations (Liu, 1994; Schubert et al., 1995; Bina and Liu, 1995; Davies, 1995; Goes et al., 2004) on mantle plumes, many of these investigations focused on one parameter in isolation and few report geoid, topographic, and heatflow anomalies. In this work, we examine the structure of thermal plumes in a set of conditions consistent with our current knowledge of the mantle, looking at the geoid, topography and heatflow anomalies predicted from the calculations. Given the range of values spanned by many of the parameters relevant to mantle convection (e.g., Table 1), we avoid reporting only those cases where the resulting plumes are consistent with the hotspot observations. Instead, we consider a range of values for each parameter that span the uncertainties associate with the parameter, noting values where the resulting plume anomalies satisfy hotspot observations as well as those that do not. It makes sense to present this in a series of steps, adding one additional parameter at a time.

METHOD

The approach that we will take is to use 2D spherical-axisymmetric calculations using the finite element code SCAM (Kellogg and King, 1997). The axis of symmetry occurs about the pole at $\theta = 0$, where θ is the co-latitude. This geometry enforces a symmetry and stability on the resulting thermal plumes. The temperature and velocity are functions of the radius, r, and the colatitude, θ, and are independent of the longitude, φ. For problems with variable viscosity, the equations for momentum and mass conservation are given by

$$-\nabla p + \nabla \cdot (\eta \dot{\varepsilon}) = RaT\hat{r} \tag{2}$$

and

$$\nabla \cdot u = 0, \tag{3}$$

where p is the dynamic pressure; η is the viscosity, which can be a function of temperature, pressure, composition and/or strain-rate; Ra is the Rayleigh number (defined in Equation 1); T is the temperature, and u is the velocity and

$$\dot{\varepsilon} = \frac{1}{2}(u_{i,j} + u_{j,i}) \tag{4}$$

is the deviatoric deformation-rate.

The conservation of energy equation in a spherical axisymmetric geometry is given by

$$\frac{\partial T}{\partial t} + u_r \frac{\partial T}{\partial r} + \frac{u_\theta}{r}\frac{\partial T}{\partial \theta} = \frac{1}{r^2}\frac{\partial}{\partial r}\left(\kappa r^2 \frac{\partial T}{\partial r}\right) + \frac{1}{r^2 \sin\theta}\frac{\partial}{\partial \theta}\left(\kappa \sin\theta \frac{\partial T}{\partial \theta}\right) + H, \tag{5}$$

where T is the temperature, t is time κ is the thermal diffusivity, u_r and u_θ are the radial and azimuthal components of velocity, and H is the rate of internal heating. Equation (5) is solved using Streamline-Upwind Petrov-Galerkin (SUPG) shape functions (Hughes, 1987) with bilinear elements. This method is second-order accurate in space.

We use an Arrhenius form for the temperature-dependent part of the viscosity law,

$$n(\hat{T}) = \eta_o \exp\left(\frac{E^*}{\hat{T} + T_o}\right) \exp\left(-\frac{E^*}{1 + T_o}\right), \tag{6}$$

where η^* is the normalized pre-exponential viscosity, $n(\hat{T})$ is the effective viscosity, $\hat{T}$ is the dimensionless temperature, and E^* is the activation energy divided by $R\Delta T$, where ΔT is the temperature scaling factor, and T_o is the temperature offset. The second exponential scales $n(\hat{T})$ so that $\eta(1.0) = \eta_o$. In these calculations we use an activation energy of 350 kJ/mole unless otherwise noted (c.f., Karato and Wu, 1993).

The method for calculating topography and geoid anomalies is described in Kiefer and Hager (1992) and King and Hager (1994). The geoid anomaly, δN, is scaled by

$$\delta N = \frac{G\rho_m \alpha \Delta T D^2}{g} \delta N' \tag{7}$$

where G is Newton's gravitational constant, ρ_m is the average mantle density, g is the acceleration due to gravity, α is the coefficient of thermal expansion, ΔT is the temperature-drop across the fluid, D is the depth of the fluid, and the values of the constants are given in Table 1. The topography anomaly, δh is given by

$$\delta h = \left(\frac{\rho_m}{\rho_s} \right) \alpha \Delta T D \delta h' \tag{8}$$

where ρ_s is the density of the surface layer.

We use a 2D, rather than a 3D geometry because of computational grid needed to ensure that our solutions are well resolved. The resolution needed before the peak geoid, topography and heatflow anomalies show signs of converging is a factor of 3 greater than the resolution used in most 3D calculations (Table 2). With temperature-dependent rheology, the issue of resolution is even more significant than it is with a constant viscosity fluid because the viscosity changes by several orders of magnitude over less than 100 km within the plume geometries in this study. Two limitations of the 2D spherical axisymmetric geometry are that we cannot consider a moving plate and the plume is stationary. Davaille and Vatterville (2005) show the effects of time-dependence on plumes in a series of tank experiments and we caution that steady-state plumes may produce larger anomalies than transient plumes. In the calculations presented here, the upwelling material carried by the plumes spreads out symmetrically beneath the top thermal boundary layer. This undoubtedly over-estimates the topographic and geoid swell for the Pacific hotspots, where some of the upwelling material should be advected in the direction of plate motion (c.f., Ribe and Christensen, 1994b). The calculations here then are more directly

comparable to hotspots over slow moving, or stationary plates; however, we do not see any reason that the general trends we find would be invalidated in three dimensions. The moving plate will advect some of the plume material in the direction of plate motion (e.g, Ribe and Christensen, 1994b) and the peak anomalies should be smaller than those calculated here. There is no correlation between the velocity of the plate and the hotspot topographic anomaly (see Sleep, 1990 Table 3).

We also present our results at steady-state conditions. While it is unlikely that the mantle is in a state of thermal equilibrium, or steady-state, presenting our results at steady-state gives us a well-defined condition to compare results from one set of calculations to another. If, for example, we chose a time early in the thermal evolution of one calculation and later in the thermal evolution of another calculation, we risk mapping changes in thermal evolution into our comparison of physical properties. We avoid this by using Picard iteration (e.g., Cuvelier et al., 1986) which solves the equations of motion for the steady-state solution (i.e., $\frac{\partial T}{\partial t} = 0$ in equation (5)). When calculations are time-dependent we use an explicit time stepping scheme and allow the solution to reach a quasi-steady or statistically steady state.

Table 2 presents the calculated maximum geoid, topography and heatflow anomalies from a typical 2D, axisymmetric calculation as a function of computational grid. The calculation has temperature-dependent rheology (e.g., equation 6), with a Rayleigh number (based on the interior viscosity) of 10^6 and uniform thermodynamic properties. While the grid resolution does not affect the overall planform of the temperature field, it has a significant impact on the values of the heatflow, geoid, and dynamic topography. Grid A (50 by 64 elements) is typical of the resolution used in many 3D spherical calculations. We present all of the results in this study using grid E (150 by 192 elements).

RESULTS

We begin by presenting a comparison of constant viscosity convection calculations in 2D Cartesian and spherical axisymmetric geometries (Figure 1). In both cases, the Rayleigh number is 10^6, there is no internal heating, the fluid is heated from below and cooled from above and the top, bottom and sides are uniform free-slip boundaries. While the assumptions is this calculation are far from the properties of the Earth, it is a mathematically well-defined starting point and corresponds to the assumptions used in the original scaling arguments used in plume theory. The most striking difference between the calculations is the internal temperature of the fluid and the temperature contrast between the upwellings and downwellings. In the Cartesian case, the volume average temperature is 0.5 with symmetric upwellings and downwellings, whereas in the spherical case, the volume average temperature is 0.14 and the upwelling is much stronger than the downwelling. In spherical geometry the upwelling most of the heat from the base of the fluid is advected up the plume tail. The difference between these calculations is largely the result of the difference in surface area between the top and bottom of the spherical shell. In the Cartesian case, the surface area of the top and bottom boundaries is the same. In the spherical case, the surface area of the bottom is approximately 1/4 of the surface area of the top $((R_{CMB}/R_{Surf})^2)$. To be in equilibrium, the total heat into the bottom shell is equal to the total heat out the top. Because of the difference in surface areas the heatflux (heat per unit area) into the bottom of the shell is much larger than the heatflux out of the top of the shell. As a result, because the thickness of the boundary layer is proportional to the heatflux, the bottom boundary layer is thicker than the top boundary layer and the upwelling caries more heat than the downwelling.

While the effects of spherical geometry are well understood (c.f., Jarvis et al., 1995; King, 1997) it is worth beginning the plume calculations by pointing out that the spherical nature

of planets favors the development of a large thermal boundary layer at the bottom of the mantle because of the difference in surface areas. It is also noteworthy that the constant viscosity convection calculation in spherical axisymmetric geometry (Figure 1) does not resemble any cartoon or model of convection in a planetary body. Further, note that it has been well established (e.g., Nataf and Richter, 1982) that temperature-dependent rheology will increase the average interior temperature with asymmetric top and bottom boundary layers. This will have the effect of creating an asymmetry in the boundary layers in Cartesian geometry, increasing the interior temperature, and decreasing the effect of the bottom thermal boundary layer in the spherical shell geometry. Thus, with temperature-dependent viscosity, or a viscous lid to simulate the effect of temperature-dependence, the difference between Cartesian and spherical shell upwellings is less dramatic than shown here. For the constant viscosity, spherical-axisymmetric shell with a Rayleigh number of 10^6, the heatflow anomaly over the plume is more than 196 mW/m^2, the peak geoid anomaly is 280 meters and the peak topographic swell anomaly is 11,000 meters.

The next step is to include temperature-dependent rheology, the subject of prior investigations, particularly with respect to starting plumes (e.g., Sleep et al., 1988; Olson et al., 1987; 1993; van Keken, 1997; Kellogg and King, 1997); however, these studies did not examine the geoid, topography and heatflow anomalies. We use equation (6) for the temperature-dependence of rheology, and now use the viscosity based on the volume averaged temperature as the viscosity in the definition of the Rayleigh number. We also include a high-viscosity shell with a thickness of 90 km and a viscosity that is 10^3 times the background viscosity to create a strong lithosphere. Kiefer and Hager (1992) show that the geoid and topography are insensitive to the viscosity of the lithosphere, as long as it is greater than 10^3 times the background viscosity.

In this case, we see a dramatic difference in the steady-state temperature field for the temperature-dependent plume calculation (Figure 2) as compared with constant viscosity calculation. The structure of the plume is largely unaffected but now a significant thermal boundary layer forms at the surface and the average internal temperature (0.43) is significantly greater than the constant viscosity case (0.14). The heatflow anomaly over this plume is just over than 16 mW/m^2, the peak geoid anomaly is approximately 142 meters, and the peak topographic swell anomaly exceeds 4,700 meters. These are still considerably larger than observations at hotspots. As the Rayleigh number increases (Table 3, rows 1-5) the geoid and topographic anomalies decrease, as has previously been shown by Kiefer and Hager (1992); however the heatflow anomaly increases, so by increasing the Rayleigh number we can not bring all of the anomalies associated with the plumes in these calculations into the range of the geophysical observations at hotspots.

We recognize that the mantle of the Earth is not strictly heated from below, but is also heated from within by the decay of radioactive elements. While the distribution of radiogenic elements may not be uniform throughout the mantle (c.f. Anderson, 2005a; 2005b) we restrict this investigation to the simplest case of uniform heat generation throughout the mantle. The next series of calculations (Figure 3) uses temperature-dependent viscosity and a volume-averaged Rayleigh number of 10^6 in spherical shell that is identical to the calculation from Figure 2, except that now a volumetric heat source term (i.e., H in equation 5) is included. We define the Rayleigh number based on the ΔT across the shell and vary the rate of internal heating (Table 3, rows 6-10). Convection with strong internal heating does not have steady-state solutions, and so here we run the calculations with an explicit time-stepping scheme until the shell achieves a quasi-steady state. With the highest rate of internal heating (1.5 mW/m^3) the

heatflow anomaly over the plume is approximately 13 mW/m^2, the maximum geoid anomaly is 16.4 meters and the maximum topographic swell anomaly is 3745 meters. This rate of internal heating is still nearly a factor of ten smaller than estimated for the present day Earth (Schubert et al., 2001); however solutions with higher rates of internal heating are strongly-time dependent, making quantitative comparisons difficult. We plot the temperature excess in the plume as a function of depth (i.e., temperature along the axis divided by the adiabatic temperature) in Figure 3D. Two effects are clear: first, the temperature excess is reduced as the amount of internal heating increases (comparing the different curves); and second, the temperature excess as a function of depth decreases throughout the lower part of the domain. This is a well-documented effect of internal heating (e.g., Bunge et al., 2001; Goes et al., 2004; Zhong, 2006). If we extrapolate the trend of the results in Table 4 to a realistic rate of internal heat generation for the Earth, the results of the plume calculations approach the range of the hotspot observations. It is important to remember that these calculations have a stagnant lid and do not have moving plates. Both of these probably contribute to the large thermal anomaly below the lithosphere. A stagnant lid is less efficient at removing heat from the interior (e.g., Gurnis, 1989); hence we do not expect to be able to use an earth-like rate of internal heat generation with stagnant lid calculations. Plate-like surface boundary conditions will cool the interior more efficiently (e.g., Gurnis, 1989) and could lead to the formation of larger instabilities at the core-mantle boundary. It is interesting to note that the width of the thermal anomaly of the plume tail does not change as the rate of internal heating increases; however the magnitude of the thermal anomaly decreases relative to the increasing average internal temperature of the shell.

We next consider the viscosity of the lower mantle. Theory shows that the geoid and dynamic topography are sensitive to the radial mantle viscosity profile and observations from

subduction environments (e.g., Hager, 1984; Chen and King, 1998), plumes (e.g., Richards et al., 1988; Kiefer and Hager, 1992), global geoid inversions using seismic tomography models (e.g., King and Masters, 1992) and glacial isostatic adjustment studies (e.g., Mitrovica, 1996) are consistent with a factor of 10-100 viscosity contrast between the upper and lower mantle. A result of the temperature-dependent rheology used in these calculations is that the viscosity of the lower mantle is actually lower than the viscosity of the upper mantle, due to the radial temperature profile. Hence, a modest radial viscosity increase with pressure would be needed to maintain a uniform viscosity with depth. Therefore, our next set of calculations (Table 3, rows 11-14) examine the effect of the lower mantle viscosity on the geoid, topography, and heatflow, using the same temperature-dependent rheology and a volume-averaged Rayleigh number of 10^6, where the viscosity in the Rayleigh number is the volume-averaged viscosity, and the value of the internal heat generation term is 0.8×10^{-12} W/kg (e.g., Table 3 row 9). To this we now add a lower mantle viscosity increase of 10, 30, and 100, a range of lower mantle viscosities consistent with subduction studies (e.g., Hager, 1984), global inversions of the flow driven by seismic velocity (e.g., King and Masters, 1992) and glacial isostatic adjustment (e.g., Mitrovica, 1996). Increasing the lower mantle viscosity decreases the peak geoid and topographic anomalies, as has been shown before (c.f., Richards et al., 1988; Kiefer and Hager, 1992); however, this also decreases the average internal temperature of the shell and increases the heatflow anomaly associated with the plume. We could lower the heatflow anomaly by increasing the rate of internal heating, which in this calculation is only about 10% of the estimated rate of internal heat generation for the mantle. This would increase the average internal temperature of the shell, reducing the temperature-drop across the bottom thermal boundary layer and the heatflow anomaly associated with the plume (Table 3, rows 11-14). However, to keep our experiments

simple and to clearly present the effect of each parameter, we did not attempt to change the viscosity and the rate of internal heating simultaneously. Because these calculations have a stagnant lid and lack plate tectonics, it will be impossible to generate completely realistic thermal conditions from these calculations.

An important aspect of the equation of state of mantle minerals is that the coefficient of thermal expansion decreases with depth (c.f., Chopelas and Boehler, 1992; Chopelas, 2000). Thus a temperature anomaly of 200° in the lower mantle will not have the same buoyancy force as the same temperature anomaly in the upper mantle. We next consider this effect by taking the calculation with a factor of 30 viscosity contrast from Table 3 (row 13) and adding a coefficient of thermal expansion of the form:

$$\alpha(r) = \alpha_o (r / r_o)^3, \tag{9}$$

where $\alpha(r)$ is the coefficient of thermal expansion as a function of depth, α_o is the surface coefficient of thermal expansion, r_o is the surface radius, and r is the radius at depth. This functional form reduces the coefficient of thermal expansion by a factor of 6.25 from the surface to the core mantle boundary. When changing the coefficient of thermal expansion, it is important to carefully consider what value of the coefficient of thermal expansion to use in the definition of the Rayleigh number. We note that we don't consider a fully self-consistent equation of state (Ita and King, 1994). While this would be more consistent, such calculations are intensive and rely on parameters that are as yet poorly constrained. In our previous work (Ita and King, 1994), we found that the primary effect of the fully self-consistent equation of state came from the variable coefficient of thermal expansion, which is not surprising because the coefficient of thermal expansion is contained in the buoyancy force term and buoyancy is the driving force of convection. We present results both where we use the surface value of the

coefficient of thermal expansion in the Rayleigh number as well as the volume-averaged coefficient of thermal expansion (Table 3, rows 15-17). These calculations become time-dependent so an explicit time stepping algorithm is used; however, the planform of the plume and anomalies remain stable in spite of the time-dependence, which takes the form of small instabilities in the boundary layers away from the central upwelling. Using the surface or the volume-averaged coefficient of thermal expansion in the Rayleigh number gives two different values of the Rayleigh number for the same calculation. Conversely, if we hold the Rayleigh number fixed, as we have been with these calculations, the two solutions with different definitions of coefficient of thermal expansion in the Rayleigh number will follow the trend of changing the Rayleigh number. The Rayleigh number based on the surface value of the coefficient of thermal expansion is larger than the Rayleigh number based on the volume averaged coefficient of thermal expansion, and the results in Table 3, rows 15-17 do indeed follow the trends for increasing the Rayleigh number that were presented in Table 3, rows 1-5.

To better illustrate the difference between the solutions, we subtract the reference field (i.e., the constant coefficient of thermal expansion calculation with temperature-dependent viscosity, a rate of internal heating of 0.8×10^{-12} W/kg, and an increase in viscosity of a factor of 30 at 660 km, i.e., the case in Table 3 with a viscosity ratio of 30, row 13) from the temperature fields from the variable coefficient of thermal expansion calculations. Figure 4a is the reference calculation temperature field with a constant coefficient of thermal expansion, temperature-dependent viscosity, a rate of internal heating of 0.8×10^{-12} W/kg, and an increase in viscosity of a factor of 30 at 660 km, i.e., the case in Table 3 with a viscosity ratio of 30). Figure 4b is the variable coefficient of thermal expansion case with a volume averaged alpha used in the definition of the Rayleigh number and Figure 4c is the temperature field from the variable

coefficient of thermal expansion with the surface value used in the definition of the Rayleigh number. While the contour plots of the fields look similar, difference can be more readily seen by looking at a temperature profile at a constant radius taken 350 km above the core mantle boundary (Figure 4d) or by looking at the difference between the reference temperature field (Figure 4a) and the variable coefficient of thermal expansion temperature fields (Figure 4e volume averaged alpha and Figure 4f surface alpha). A decrease in the coefficient of thermal expansion with increasing pressure, coupled with the increase in lower mantle viscosity has a profound influence on the thermal structure of the plume. First, the using the surface value of the coefficient of thermal expansion (Figure 4c, 4f) leads to an interior that it hotter than the reference case, although the structure of the plume remains almost unchanged. The difference is dominated by the increase in the Rayleigh number that results from using the high surface value of the coefficient of thermal expansion and it is difficult to see any changes in the plume. The calculation where the volume-averaged coefficient of thermal expansion is used (Figure 4b, 4e), the effect on the plume is still pronounced; the bottom-half of the plume conduit (and the basal thermal boundary layer) is hotter (by approximately 200 degrees maximum) and broader (by approximately 200 km in diameter) than the constant coefficient of thermal expansion calculation, while the top half of the plume conduit is cooler and more narrow than the constant coefficient of thermal expansion calculation. A larger temperature contrast in the lower mantle is required to achieve a similar magnitude buoyancy force because of the reduction in the coefficient of thermal expansion with depth and we observe that the plume is hotter in the lower mantle and cooler in the upper mantle, which compensates, at least partially, for the change in the coefficient of thermal expansion with depth. The temperatures in the plume tail for the variable coefficient of thermal expansion cases are significantly lower than the reference case.

Once again, the geoid, topography and heatflow are significantly larger (in most cases by a factor of two) than the upper limit of the hotspot observations (Table 3, rows 15-17).

While the effect of phase transformations has been included in a number of previous investigations (e.g., Davies, 1995; Schubert et al., 1995; Christensen, 1995; Farnetani and Richards, 1994), as the planform of the plumes has changed significantly with the inclusion of a variable coefficient of thermal expansion, for completeness we consider the effect of an endothermic phase transformation here. The effect of the exothermic olivine to wadslayite transformation (which occurs at approximately 410-km depth) will enhance the vertical motion of the plume in the upper mantle (c.f., Christensen, 1995) and we do not include it here. We consider Clapeyron slopes of -1.0, -2.0 and -2.8 MPa/°K for the phase transformation from ringwoodite to perovskite plus ferropericlase (which occurs at approximately 660 km). We implement the phase transformation using the phase function formulation described by Christensen (1995). This assumes that we can treat the 660 km discontinuity (or more broadly the bottom of the transition zone) as a single uni-variant phase change. Deuss et al. (2006) show that *PP* and *SS* precursors show different behavior in the same location, which can not be explained by temperature variations in the region and requires additional phase transformations and/or compositional differences. Several studies have considered the effect of temperature on the endothermic ringwoodite to spinel plus ferropericlase boundary, showing the effect in slabs and plumes could be different (Liu, 1994; Bina and Liu, 1995; Davies, 1995). In spite of potential problems, the formulation we use is a common formulation in numerical calculations of mantle convection and recognizing the potential limitation we forge ahead. The current best estimate of the Clapeyron slope for this phase transformation is -2.8 MPa/°K (Hirose, 2002). Because the garnet component of the mantle undergoes a broad, nearly-continuous set of phase

transformations through the transition zone, the effect of the garnet component of the mantle is approximated by reducing the Clapeyron slope of the olivine system by a mass-weighted average of the two components. Thus the most appropriate value of the Clapeyron slope is probably between -1.0 and -2.0 MPa/°K. The heatflow, geoid, and topographic anomalies are presented as a function of the Clapeyron slope in Table 3, rows 18-21. The influence of the Clapeyron slope is most pronounced on the geoid because the thermal structure of the plumes is most affected by the phase change in the transition zone and the geoid includes a term that is the integral of the density anomalies with depth. As with the previous calculations, the magnitude of the swell observations from these plume calculations are larger (generally by a factor of two) than the upper limit of the hotspot observations.

We finally examine a stably-stratified D" layer. There have been speculations that the D" layer is both a chemical layer (e.g., Christensen and Hofmann, 1994; Farnetani, 1997) and a stably-stratified layer due to the post-perovskite phase transformation (c.f., Matyska and Yuen, 2005). In order to model a stably-stratified D" layer, we take a simple approach and use a high viscosity layer for the bottom 90 km of the shell. While we do not intend to suggest that the lowermost mantle has such a high viscosity, the high viscosity layer acts like a stable chemical or phase change boundary near the boundary. The inclusion of a stably-stratified layer has a profound effect on both the thermal structure of the plume and the average internal temperature of the fluid. This is best illustrated by comparing calculations with and without the stably-stratified layer that have variable coefficient of thermal expansion, an increase in viscosity of a factor of 30 at 660 km, a rate of internal heating of 0.8×10^{-12} W/kg and a Clapeyron slope of -2.8 MPa/°K (e.g., Table 3, rows 18-21). The difference in internal temperature of 0.42 for the no layer calculation (Figure 5a) versus 0.32 for the calculation with a layer is immediately apparent

from the color shading (Figure 5b); however the difference between the magnitudes of the thermal anomalies of the plumes is also striking and potentially more important. This is reflected in the reduction in the heat flow anomaly from 27 to 15 mW/m^2 for the no layer and layer calculations respectively. The geoid decreases from 28 to 25 meters for no layer and layer respectively while the topography decreases from 3168 to 2358.1 meters for the no layer and layer calculations respectively. This result is consistent with the findings of Farnetani (1997) and Goes et al. (2004). Note that the effect of a thin layer at the base of the mantle is different than the effect of a thicker layer in the mid-lower mantle or transition zone (e.g., Wen and Anderson, 1997a; 1997b; Kellogg et al., 1999; Nakagawa and Tackley, 2004). This could have a significantly different effect on the planform of lower thermal boundary layer instabilities leading to broad superplumes that may not be directly related to hotspots.

As this represents the final parameter in our modeling exercise, we wish to explore whether we can push these plume calculations further by varying the rate of internal heat generation further to bring the geophysical anomalies more in line with the hotspot observations. It is important to recall that the value of internal heat generation we have been using is significantly smaller than realistic estimates for the Earth, so by increasing this value, we are still well within the estimated parameter range of Earth-like internal heating. We also consider calculations with internal heat generation rates of 0.8×10^{-12} W/kg and 2.4×10^{-12} W/kg, which represents approximately 30% of the estimated mantle heat production rate, and 4.8×10^{-12} W/kg, which represents approximately 70% of the estimated mantle heat production rate. The resulting peak geoid, topography and heatflow anomalies for all three deep layer calculations are shown in Table 3, rows 22-24. The temperature field from the calculation with an internal heat generation rate of 4.8×10^{-12} W/kg is shown in Figure 5c. While there is clear evidence in

Figure 5c that small-scale convection the upper mantle is inhibited by the phase transformation away from the axis where the upwelling plume forms, the central upwelling plume still penetrates the phase boundary. The resulting geoid, topographic and heat flow anomalies illustrate that it is very challenging (at best) to produce thermal plumes that are consistent with the geophysical observations at hotspots, a result consistent with the recent work of Goes et al. (2004).

DISCUSSION

While the geometry of the axisymmetric calculations shown here ensures that the resulting thermal structures will take the form of plumes, both theory (e.g. Busse, 1975; Busse and Riahi, 1982) and 3D spherical calculations (e.g., Bercovici et al., 1989; Tackley et al., 1993; 1994; Bunge et al., 1996; 1997; Zhong, 2006) show that plumes are the upwelling planform of spherical shell convection. While it is possible that the lower mantle has deep instabilities that more closely resemble broad superplumes (e.g., Nakagawa and Tackley, 2004), the observed broad structures could also be consistent with clusters of plumes (e.g., Schubert et al., 2004) or there could be a mixed mode of superplumes (or domes) and more conventional plumes (e.g., Davaille, 1999; Courtillot et al., 2003). The question addressed here is under what conditions are the thermal plumes in these calculations consistent with the observations at hotspot swells. The straightforward answer is that the geoid, topography and heatflow anomalies at hotspots are challenging to match with thermal plume calculations. While we have avoided 'tuning' these models by continuing to vary the parameters to get a calculation that is consistent with the observations, the point is that if hotspots are the result of thermal plumes, these plumes must be weaker than the plumes in our calculations. It is important to point out that computational studies are showing that the structure of instabilities from the core mantle boundary in more

complex fluid systems are diverse and do not always fit the traditional plume model (e.g., Farnetani and Samuel, 2005; Lin and van Keken, 2006b).

Perhaps the most interesting result from this sequence of calculations is the change in the plume conduit shape with the inclusion of pressure-dependent coefficient of thermal expansion, as shown in Figure 4. The plume conduit becomes broader at the base of the mantle and smaller in the upper mantle compared to the constant coefficient of thermal expansion calculation. The deep mantle has less thermal buoyancy for a given thermal anomaly, hence instabilities at the base of the mantle must be larger than they would be with a constant coefficient of thermal expansion to achieve the same buoyancy force. The resulting calculations are time-dependent and the structure of the plume, particularly the plume conduit is more variable with depth. The broadening of the plume conduit with depth has interesting implications for seismic imaging. While this effect is modest, in the overall picture it has several important implications for mantle plumes. One of the difficulties encountered applying mantle plumes to hotspot volcanism is that the estimated temperature contrast at the core mantle boundary leads to plumes upwellings that are too hot when compared with the excess temperatures estimated from hotspot related volcanism. This effect is reduced to some extent by the subadiabaticity of the lower mantle (Bunge et al., 2001; Zhong, 2006). The variable coefficient of thermal expansion reduces the temperature in the uppermost part of the plume, compared with estimates of plume excess temperature that come from uniform coefficient of thermal expansion calculations. Second, previous work has shown that the impact of the endothermic phase transformation becomes more pronounced when coupled with a decrease in the coefficient of thermal expansion (Ita and King, 1994). Previous investigations of the interactions of plumes and an endothermic phase transformation have found little or no evidence that the ringwoodite to perovskite plus

ferropericlase phase change will inhibit a rising plume (Schubert et al., 1995) and our results confirm that this is still the case, even when we include the pressure effect of the coefficient of thermal expansion.

When we include a stable layer at the base of the mantle, the geoid, topographic and heatflow anomalies associated with the plumes approach the upper limit of the hotspot observations. There have been speculations that the D" layer is both a chemical layer (e.g., Christensen and Hofmann, 1994; Farnetani, 1997) and a stably-stratified layer due to a phase change (c.f., Matyska and Yuen, 2005). While our approach does not include all of the relevant physics of these hypotheses, which have been studied in more detail by others, it illustrates the important effect that a stably-stratified layer can have on the thermal structure of plumes. This stably-stratified layer at the base of the mantle leads to a thick, stable conductive thermal layer with a smaller, active thermal boundary layer above it. The upwelling plume that forms has a smaller temperature-contrast compared with the surrounding mantle than an identical calculation without a stably-stratified layer at the base of the mantle. It is possible that if we were able to perform calculations with even larger rates of internal heating, we could achieve a similar plume thermal structure without a stable layer at the base of the mantle, so we are cautious that this may be the result of a limitation of our calculations.

The next result is rather obvious, there must be a thermal boundary layer at the core-mantle boundary in order for deep-mantle plumes to form there. For example, in the calculation with 100% internal heating (Figure 3C), no upwelling plume forms. The best estimate of the temperature mismatch between extrapolating from the inner core boundary through the core to the base of the mantle and extrapolating the geotherm through the mantle gives a 1000-1800 degree temperature drop across the core mantle boundary (Anderson, 2002). This range depends

on a number of assumptions; however, given the large value, it seems challenging to completely eliminate it. . In fact, our results suggest that this difference is currently too large to be contained in a thermal boundary layer without somehow stabilizing the layer (either chemically or by a phase transformation) and isolating part of the temperature contrast, as in our calculations with a stable D" layer (Figure 5C). This result is also consistent with the findings of Goes et al. (2004), Farnetani (1997), and Lin and van Keken (2006a). The large temperature contrast between the core and mantle forces the consideration of some kind of thermal boundary layer instability and the alternative to the kinds of plume structures shown here would be broad superplume structures (e.g., Nakagawa and Tackley, 2002; Anderson, 2005a; 2005b). We do not investigate this mode of convection here.

Additionally, without a stiff, viscous lid, the resulting geoid, topographic and heatflow anomalies are impossible to reconcile with observations (e.g., Figure 1). While this is a well-known result (e.g., Kiefer and Hager, 1992), the calculations here reinforce the importance of a viscous lid. Yet, because hotspots occur on all types of lithosphere from cratons to ridges and we do not see a significant correlation between the hotspot anomalies (e.g,, geoid, topography, and heaflow) and the type of lithosphere, we do not consider the strength or thickness of the lithosphere to be primary controlling factor in hotspot swell properties.

We have not reported the width of the plumes from these calculations, in large part because in order to compare these results with seismic images, we need to convert the temperature anomalies to seismic velocity anomalies. Our results are comparable with those of Goes et al. (2004), and we estimate that our calculations will produce seismic anomalies in the range of 500-900 km diameter in the lower mantle. This is wider than the seismic images presented by Montelli et al. (2003) and also the plume tails from typical cartoons and

calculations of mantle plumes. Increasing the Rayleigh number of the calculation would decrease the width of the boundary layers (c.f., Schubert et al., 2001); however increasing the Rayleigh number will also increase the heatflow anomaly (c.f., Table 3, rows 1-5).

One parameter that we have not considered is variable thermal conductivity and the possibility of radiative thermal conductivity (Hoffmeister, 1999). Convection calculations show that variable thermal conductivity leads to more sluggish convection in the lower mantle and broader, stronger plumes (e.g., Dubuffet and Yuen, 2000; van den Berg et al., 2001). The non-linear interaction between variable viscosity and thermal conductivity with phase transformations is being investigated by a number of researchers and it would not be possible to properly add variable thermal conductivity and produce meaningful results here because of the non-linear feedback. At the present time, it appears that variable thermal conductivity will produce larger anomalies over plumes, making it more difficult to match the hotspot observations with plume calculations; however this requires further investigation.

CONCLUSIONS

There are several scenarios under which deep-mantle plumes would not form: this either requires a core heatflux that is so small that no significant boundary layer forms at the base of the mantle, or a compositional, phase change and/or combination of pressure dependent effects give rise to broad, deep superplumes (e.g., Kellogg et al., 1999; Davaille, 1999; Monneareau and Yuen, 2002; Courtillot et al., 2003; Nakagawa and Tackley, 2004). We do not evaluate superplume like models here, although superplume models require either coupling with the upper mantle to explain hotspots (e.g., Courtillot et al., 2003) or a mechanism independent of superplumes (e.g., Anderson, 2005a; 2005b). We find thermal plume cases that produce unacceptably large geophysical anomalies, including cases with constant mantle viscosity or

temperature-dependent rheology and no internal heat generation, which are easy to rule out as geophysically unreasonable. However, most of the calculations here have geophysical anomalies that are a factor of two to four larger than hotspot observations, and only approach the upper limit of the range of observations at hotspots as we include depth-dependent mantle viscosity, a significant rate of internal heat generation, a depth-dependent coefficient of thermal expansion, and a stable D" layer. In a strict formal sense, we have not been able to produce hotspot geophysical anomalies with thermal plumes. We speculate that the inability to include mobile plates in the spherical axisymmetric domain is a significant limitation because 1) upwelling material ponds beneath the boundary layer and is not advected away from the plume by the plate-scale flow (c.f., Ribe and Christensen, 1994b), and 2) the stagnant-lid mode of convection does not allow for realistic cooling of the lithosphere (c.f., Gurnis, 1989). Recent 3D spherical results with a compressible mantle are able to match plume heatflux and plume excess temperature (Zhong, 2006). The 2D axisymmetric geometry also enforces a symmetry on the fluid system that could influence our results and the steady-state assumption, necessary to compare one result with another without confusing time-dependent effects with material property dependent effects, could be important. Several recent computational studies have shown that with more Earth-like parameters instabilities from the core-mantle boundary are time dependent and some of the features of the plume model (e.g., large heads and long lived tails) are not always present in every instability (Farnetani and Samuel, 2005; Lin and van Keken, 2006). We also point out that the calculations we present are incompressible. In a compressible fluid with variable coefficient of thermal expansion the temperature contrast at the base of the fluid may be significantly larger than the temperature contrast as the plume nears the surface (e.g., Monnererau and Yuen, 2002)

which could reduce the thermal anomaly associated with plumes; however, these calculations also often lead to partially-layered flows with broad superplumes,.

Perhaps the most interesting result is the change in the plume conduit (i.e., tail) shape with the inclusion of pressure-dependent coefficient of thermal expansion. The plume tail is broader at the base of the mantle and the overall thermal anomaly in the plume tail at any given depth is smaller than in the constant coefficient of thermal expansion calculations. We speculate that the width of the thermal structures in these calculations of approximately 950 km in diameter 300-500 km above the core mantle boundary, should be resolvable by seismic imaging, especially when accounting for the fact that the seismic anomaly will be broader than the thermal anomaly (c.f., Goes et al., 2004). The shape of the plumes in these calculations differs from the lollipop-like shape seen in tank experiments and we would expect the broader plume tails in these calculations should be resolvable by seismic imaging techniques.

Finally, an increase in mantle viscosity with depth, decrease in coefficient of thermal expansion with depth, a significant fraction of internal heating and a stably-stratified D" are all critical to producing plumes with geophysical observations of heatflow, geoid and topographic anomalies that approach the range of the hotspot observations. Uniform-property plume calculations are impossible to reconcile with the hotspot observations. This is important because many of the simple scaling arguments used in plume theory are based on such simple uniform property assumptions. Given the uncertainties in the important parameters, it is not possible to say that these calculations either prove or rule-out mantle plumes as the source of hotspot anomalies. What is clear from these calculations is that the complexities of the mantle rheology and equation of state reduce what would otherwise be enormous anomalies associated with mantle plumes. The results here are best interpreted in terms of understanding how individual

parameters affect observable geophysical anomalies rather than taking any specific calculation as a `best model for mantle plumes.'

Acknowledgements

We thank Don L. Anderson, Hans-Peter Bunge, Walter Kiefer, Gillian Foulger and Donna Jurdy for helpful and thoughtful reviews. The ideas here benefited from discussions at the Great Plume Debate (Fort William, Scotland, September, 2005). The GMT software package (Wessel and Smith, 1991) was used in this work and is gratefully acknowledged. Support from NSF EAR-0207222 and NASA NAG5-13371 is acknowledged.

REFERENCES

Allen, R.M., Nolet, G., Morgan, W.J., Vogfjord, K., Bergsson, B.H., Erlendsson, P., Foulger, G.R., Jakobsdottir, S. Julian, B. R., Pritchard, M., Ragnarsson, S., and Stefansson, R., 2002, Imaging the mantle beneath Iceland using integrated seismological techniques: Journal of Geophysical Research, v. 107, B8, p. 2325, doi: 10.1019/2001JB000595.

Allen, R. M., and Tromp, J., 2005, Resolution of regional seismic models: Squeezing the Iceland anomaly: Geophysical Journal International, v. 161, p. 373-386.

Anderson, D. L., 2005a, Scoring hotspots: the plume and plate paradigms, in: Foulger, G. R., Natland, J,. H., Presnall, D. C., Anderson, D. L., Plates, Plumes, and Paradigms, Geological Society of Amererica Special Publication, v. 388, p. 31-54.

Anderson, D. L. 2005b. Self-gravity, self-consistency, and self-organization in geodynamics and geochemistry, in Earth's Deep Mantle: Structure, Composition, and Evolution, Eds. R.D. van der Hilst, J. Bass, J. Matas & J. Trampert, AGU Geophysical Monograph Series, v. 160, p. 165-186.

Anderson, D. L. and Schramm, K. A., 2005, Global Hotspot Maps, in Plates, Plumes & Paradigms, Foulger, G.R., Natland, J.H., Presnall, D.C, and Anderson, D.L., eds., Boulder, CO, Geological Society of America, Special Paper 388, p. 19-29.

Anderson, O. L., 2002, The power balance at the core-mantle boundary: Physics of Earth and Planetary Interiors, v. 131, p. 1-17.

Bercovici, D., Schubert, G., Glatzmaier, G. A., and Zebib, A., 1989, Three- dimensional thermal convection in a spherical shell: Journal of Fluid Mechanics, v. 206, p. 75-104.

Bijwaard, H. and Spakman, W., 1999, Tomographic evidence for a narrow whole mantle plume below Iceland: Earth and Planetary Science Letters, v. 166, p. 121-126.

Bina, C. R., and Liu, M., 1995, A note on the sensitivity of mantle convection models to composition dependent phase relations: Geophysical Research Letters, v. 22, p. 2565-2568.

Buffett, B.A., 2003, Thermal state of the Earth's core: Science, v. 299, p. 1675--1677.

Bunge, H.-P., Ricard, Y., and Matas, J., 2001, Non-adiabaticity in mantle convection: Geophysical Research Letters, v. 28, p. 879-882.

Bunge, H.-P., Richards, M.A. and. Baumgardner, J.R., 1996, Effect of depth-dependent viscosity on the planform of mantle convection: Nature, v. 379, p. 436-438.

Bunge, H.-P., Richards, M.A. and. Baumgardner, J. R, 1997, A sensitivity study of three-dimensional spherical mantle convection at 10**8 Rayleigh number: Effects of depth-dependent viscosity, heating mode, and an endothermic phase change: Journal of Geophysical Research, v. 102, p. 11, 991-12,008.

Burke, K. and Wilson, J.T., 1976, Hotspots on the Earth's surface: Scientific American, v. 235, p. 46-57.

Busse, F.H., 1975, Patterns of convection in spherical shells: Journal of Fluid Mechanics, v. 72, p. 67-85.

Busse, F.H., and Riahi, N.,1982, Patterns of convection in spherical shells, Part 2: Journal of Fluid Mechanics, v. 123, p. 283-301.

Chandrasekhar, S., 1961, Hydrodynamic and Hydromagnetic Stability: Oxford, Clarendon Press, 652 p.

Chen, J., and King, S.D., 1998, The influence of temperature and depth dependent viscosity on geoid and topography profiles from models of mantle convection: Physics of Earth and Planetary Interiors, v. 106, p. 75-91.

Christensen, U.R., 1995, Effects of phase transitions on mantle convection: Annual Reviews of Earth and Planetary Science, v. 23, p.65-88.

Chopelas, A. 2000, Thermal expansivity of mantle relevant magnesium silicates derived from vibrational spectroscopy at high pressure: American Mineralogist, v. 85, p. 270-278.

Chopelas, A., and Boehler, R., 1992, Thermal expansivity in the lower mantle: Geophysical Research Letters, v. 19, p. 1983-1986.

Christensen, U.R., and Hofmann, A.W., 1994, Segregation of subducted oceanic crust in the convecting mantle: Journal of Geophysical Research, v. 99, p. 19,867-19,884.

Courtillot, V., Davaille, A., Besse, J., Stock, J., 2003, Three distinct types of hotspots in the Earth's mantle, Earth and Planetary Science Letters, v. 205, p. 295-308.

Crough, S.T., and Jurdy, D.M., 1980, Subducted lithosphere, hotspots, and the geoid: Earth and Planetary Science Letters v. 48, p. 15-22.

Crough, S.T., 1983, Hotspot swells: Annual Reviews of Earth and Planetary Science, v. 11, p. 165-193.

Cuvelier, C., Segal, A., and van Steenhoven, A.A., 1986, Finite Element Methods and the Navier-Stokes Equations: D. Reidel, Norwell, Mass. 483 p.

Davaille, A., 1999, Simultaneous generation of hotspots and superswells by convection in a heterogeneous planetary mantle: Nature, v. 402, p. 756-760.

Davaille, A., and Vatterville, J., 2005, On the transient nature of mantle plumes: Geophysical Research Letters, v. 32, L14309, doi:10.1029/2005GL023029.

Davies, G.F., 1995, Penetration of plates and plumes though the mantle transition zone: Earth and Planetary Science Letters. v. 133, p. 507-516.

Davies, G.F., 1980, Thermal histories of convective Earth models and constraints on radiogenic

heat production in the Earth: Journal of Geophysical Research, v. 85, p. 2517-2530.

Davies, G.F., 1988, Ocean bathymetry and mantle convection; 1, Large-scale flow and hotspots: Journal of Geophysical Research, v.93, p. 10,467-10,480.

Davies, G. F., and Richards, M.A., 1992, Mantle convection: Journal of Geology, v. 100, p. 151-206.

DeLaughter, J., Stein, C.A., and Stein, S., 2005, Hotspots: a view from the swells, *in* Foulger, G.R., Natland, J., Presnall,D.C., and Anderson, D.L., (eds.), Plates, plumes, and paradigms: Geological Society of American Special Paper, v. 388, p. 257-278.

Deuss, A., Redfern, S. A., Chambers, K., and Woodhouse, J. H., 2006, The nature of the 660-kilometer discontinuity in Earth's mantle from global seismic observations of PP precursors: Science, v. 311, p. 198-201.

Dubuffett, F. and Yuen, D.A., 2000, A thick pipe-like heat-transfer mechanism in the mantle: Nonlinear coupling between 3-D convection and variable thermal conductivity: Geophysical Research Letters, v. 27, p. 17-20.

Dziewonski, A.M. and D.L. Anderson, 1981, Preliminary reference earth model (PREM): Physics of Earth and Planetary Interiors, v. 25, p. 297-356,

Farnetani, C.G., 1997, Excess temperature of mantle plumes; the role of chemical stratification across D": Geophysical Research Letters, v. 24, p. 1583-1586.

Farnetani, C.G., and Richards, M.A., 1995, Thermal entrainment and melting in mantle plumes: Earth and Planetary Science Letters. v. 136, p. 251-267.

Farnetani, C.G., and Richards, M.A., 1994, Numerical investigations of the mantle plume initiation model for flood basalt events: Journal of Geophysical Research, v. 99, p. 13,813-13,833.

Farnetani, C.G., Richards, M.A., and Ghiorso, M.S., 1996, Petrological models of magma evolution and deep crustal structure beneath hotspots and flood basalt provinces: Earth and Planetary Science Letters, v. 143, p. 81-94.

Farnetani, C.G., and Samuel, H., 2005, Beyond the thermal plume paradigm: Geophysical Research Letters, v. 32, L07311, doi:10.1029/2005GL022360.

Foulger, G.R., Pritchard, M.J., Julian, B.R., Evans, J.R., Allen, R.M., Nolet, G., Morgan, W.J., Bergsson, B.H., Erlendsson, P., Jakobsdottir, S., Ragnarsson, S., Stefansson, R., and Vogfjord, K., 2000, The seismic anomaly beneath Iceland extends down to the mantle transition zone and no deeper: Geophysical Journal International, v. 142, p. F1-F5.

Goes, S., F. Cammarano, and U. Hansen, 2004, Synthetic seismic signature of thermal mantle plumes: Earth and Planetary Science Letters, v. 218, p. 403-419.

Griffiths, R.W., 1986, Thermals in extremely viscous fluids: Journal of Fluid Mechanics, v. 166, p. 115-138.

Griffiths, R.W., and Campbell, I.H., 1990, Stirring and structure in mantle starting plumes: Earth and Planetary Science Letters, v. 99, p. 66-78.

Griffiths, R.W. and I.H. Campbell, 1991, On the dynamics of long-lived plume conduits in the convecting mantle: Earth and Planetary Science Letters. v. 103, p. 214-227.

Gurnis, M., 1989, A reassessment of the heat transport by variable viscosity convection with plates and lids: Geophysical Research Letters, v. 16, p. 179-182.

Hager, B.H., 1984, Subducted slabs and the geoid: Constraints on mantle rheology and flow: Journal of Geophysical Research, v. 89, p. 6003-6016.

Harris, R.N., Von Herzen, R.P., McNutt, M.K., Garven, G., and Jordahl, K., 2000, Submarine hydrogeology of the Hawaiian archipelagic apron; 1, heat flow patterns north of Oahu

and Maro Reef: Journal of Geophysical Research, v. 105, p.21,353-21,369.

Hill, R.I., Campbell, I.H., Davies, G.F., and Griffiths, R.W., 1992, Mantle plumes and continental tectonics: Science, v. 256, p. 186-193.

Hirose, K., 2002, Phase transitions in pyrolitic mantle around 670-km depth: Implications for upwelling of plumes from the lower mantle: Journal of Geophysical Research, v. 107, p. 2078.

Hofmeister, A.M., 1999, Mantle values of thermal conductivity and the geotherm from phonon lifetimes: Science, v. 283, p. 1699-1706.

Humphreys, E. D., Dueker, K. G., Schutt, D. L., Smith, R. B., 2000, Beneath Yellowstone: evaluating plume and nonplume models using teleseismic images of the upper mantle: GSA Today, v. 10, p. 1-7.

Hughes, T.J.R., 1987; The Finite Element Method: Linear static and dynamic finite element analysis: Englewood Cliffs, New Jersey, Prentice Hall, 803 p.

Ita, J.J., and King, S.D., 1994, The sensitivity of convection with an endothermic phase change to the form of governing equations, initial conditions, aspect ratio, and equation of state: Journal of Geophysical Research, v. 99, p. 15,919-15,938.

Jarvis, G.T., Glatzmaier, G.A., and Vangelov, V.I., 1995, Effects of curvature, aspect ratio and plan form in two- and three-dimensional spherical models of thermal convection: Geophysical and Astrophysical Fluid Dynamics, v. 79, p. 147-171.

Karato, S., and Wu, P., 1993, Rheology of the upper mantle: a synthesis: Science, v. 260, p. 771-778.

Kellogg, L.H., Hager, B.H., and van der Hilst, R.D., 1999, Compositional stratification in the deep mantle: Science, v. 283, p. 1881-1884.

Kellogg, L.H., and King, S. D., Effect of mantle plumes on the growth of D" by reaction between the core and the mantle: Geophysical Research Letters, v. 20, p. 379-382.

Kellogg, L.H., and King, S.D., 1997, The effect of temperature dependent viscosity on the structure of new plumes in the mantle: Results of a finite element model in a spherical, axisymmetric shell: Earth and Planetary Science Letters, v. 148, p. 13-26.

Kiefer, W.H., and Hager, B.H., 1992, Geoid anomalies and dynamic topography from convection in cylindrical geometry: Applications to mantle plumes on Earth and Venus: Geophysical Journal International, v. 108, p. 198-214.

King, S.D., 1997, Geoid and topographic swells over temperature-dependent thermal plumes in spherical-axisymmetric geometry: Geophysical Research Letters, v. 24, p. 3093-3096, 1997.

King, S.D., and B.H. Hager, 1994, Subducted slabs and the geoid: 1) Numerical calculations with temperature-dependent viscosity: Journal of Geophysical Research, v. 99, p. 19,843-19,852.

King, S. D., and Masters G., 1992, An inversion for radial viscosity structure using seismic tomography: Geophysical Research Letters, v. 19, p. 1551-1554.

King, S.D., and Ritsema, J., 2000, African hotspot volcanism: Small-scale convection in the upper mantle beneath cratons: Science, v. 290, p.1137-1140.

Lin, S.-C., and van Keken, P. E., 2006a, Dynamics of thermochemical plumes: 1. Plume formation and entrainment of a dense layer: Geochemistry, Geophysics Geosystems, v. 7, Q02006.

Lin, S.-C., and van Keken, P. E., 2006b, Dynamics of thermochemical plumes: 2. Complexity of plume structures and its implications for mapping mantle plumes: Geochemistry,

Geophysics Geosystems, v. 7, Q02006.

Liu, M., 1994, Asymmetric phase effects and mantle convection patterns: Science, v. 264, p. 1904 -1907.

Matyska, C., and Yuen, D.A., 2005, The importance of radiative heat transfer on superplumes in the lower mantle with the new post-perovskite phase change: Earth and Planetary Science Letters, v. 234, p. 71-81.

Mitrovica, J.X., 1996, Haskell (1935) revisited: Journal of Geophysical Research, v. 101, p. 555-569.

Montelli, R., Nolet, G., Dahlen, F.A., Masters, G., Engdahl, E.R., and Hung, S.H., 2003, Finite-frequency tomography reveals a variety of plumes in the mantle: Science, v. 303, p. 338-343.

Monnereau, M., and Yuen, D. A., 2002, How flat is the lower-mantle temperature gradient?: Earth and Planetary Science Letters, v. 202, p. 171-183.

Morgan, W.J., 1971, Convection plumes in the lower mantle: Nature, v. 230, p. 42-43.

Nakagawa, T., and Tackley, P. J., 2004, Thermo-chemical structure in the mantle arising from a three-component convective system and implications for geochemistry: Physics of Earth and Planetary Interiors, v. 146, p. 125-138.

Nataf, H.C., and Richter, F.M., 1982, Convection experiments temperature-dependent viscosity and the thermal evolution planets: Physics of Earth and Planetary Interiors, v. 29, p. 320-329.

Nataf, H.C., and Van Decar, J., 1993, Seismological detection of a mantle plume?: Nature, v. 364, p. 115-120.

Olson, P., and Singer, H., 1985, Creeping plumes: Journal of Fluid Mechanics, v. 158, p. 511-

531.

Olson, P.L., Schubert, G., and Anderson, C., 1987, Plume formation in the D"-layer and the roughness of the core-mantle boundary: Nature, v. 327, p. 409-415.

Olson, P.L., Schubert, G., and Anderson, C., 1993, Structure of axisymmetric plumes: Journal of Geophysical Research, v. 98, p. 6829-6844.

Ratcliff, J.T., Schubert, G., and Zebib, A., 1995, Three-dimensional variable viscosity convection of an infinite Prandtl number Bousinessq fluid in a spherical shell: Geophysical Research Letters, v. 22, p. 2227-2230.

Ratcliff, J.T., Schubert, G., and Zebib, A.,1996, Effects of temperature-dependent viscosity on thermal convection in a spherical shell.: Physica D, v. 97, p. 242-252.

Ribe, N.M., and Christensen, U.R., 1994, 3-Dimensional modeling of plume-lithosphere interaction : Journal of Geophysical Research v. 99, p. 669-682.

Ribe, N.M., and Christensen, U.R., 1994, Melt generation by plumes; a study of Hawaiian volcanism: Journal of Geophysical Research, v. 99, p. 669-682.

Richards, M.A., and Hager, B.H., 1989, Effects of lateral viscosity variations on long-wavelength geoid anomalies and topography: Journal of Geophysical Research, v. 94, p. 10,299-313.

Richards, M.A., Hager, B.H., and Sleep, N.H., 1988, Dynamically supported geoid highs over hotspots: Observation and theory: Journal of Geophysical Research, v. 93, p. 7690-7708.

Ritsema, J., and Allen, R.M., 2003, The elusive mantle plume: Earth and Planetary Science Letters, v. 207, p. 1-12.

Safronov, V.S., 1978, The heating of the Earth during its formation: Icarus, v. 33, p. 3-12.

Samuel, H., and Farnetani, C.G., 2003, Thermochemical convection and helium concentrations

in mantle plumes: Earth and Planetary Science Letters, v. 207, p. 39-56.

Sandwell, D., Anderson, D. L., and Wessel, P., 2005, Global Tectonic Maps, in Plates, Plumes & Paradigms, Foulger, G.R., Natland, J.H., Presnall, D.C, and Anderson, D.L., eds., Boulder, CO, Geological Society of America , Special Paper 388, p.1-10.

Schubert, G., 1979, Subsolidus convection in the mantles of terrestrial planets: Annual Reviews of Earth and Planetary Science, v. 7, p. 289-342.

Schubert, G., Anderson, C. and Goldman, P., 1995, Mantle plume interaction with an endothermic phase change: Journal of Geophysical Research, v. 100, p. 8245-8256.

Schubert, G., Masters, G., Olson, P., and Tackely, P., 2004, Superplumes or plume clusters?: Physics of Earth and Planetary Interiors, v. 146, p. 147-162.

Schubert, G., Turcotte, D.L., and Olson, P., 2001, Mantle Convection in the Earth and Planets, Cambridge, Cambridge University Press, 940 p.

Schott, B., and Yuen, D. A., 2004, Influences of dissipation and rheology on mantle plumes coming from the D”-layer: Physics of Earth and Planetary Interiors, v. 146, p. 139-145.

Sleep, N.H., 1996, Lateral flow of hot plume material ponded at sublithospheric depths: Journal of Geophysical Research, v. 101, p. 28,065 -28,083.

Sleep, N.H., 1994, Lithospheric thinning by midplate mantle plumes and thermal history of hot plume material ponded at sublithospheric depths: Journal of Geophysical Research, v. 99, p. 9327-9343.

Sleep, N.H., 1992, Time dependence of mantle plumes: Some simple theory: Journal of Geophysical Research, v. 97, p. 20,007-20,019.

Sleep, N.H., 1990, Hotspots and mantle plumes: Some phenomenology: Journal of Geophysical Research, v. 95, p. 6715-6736.

Sleep, N.H., Richards, M.A., and Hager, B.H., 1988, Onset of mantle plumes in the presence of preexisting convection: Journal of Geophysical Research, v. 93, p. 7672-7689.

Stacey, F.D., and Loper, D.E., 1983, The thermal boundary layer interpretation of D" and its role as a plume source: Physics of Earth and Planetary Interiors, v. 33, p. 45-55.

Tackley, P.J., Stevenson, D.J., Glatzmaier, G.A. and, Schubert, G., 1993, Effects of an endothermic phase transition at 670 km depth in a spherical model of convection in the Earths mantle: Nature, v. 361, p. 699-704.

Tackley, P.J., Stevenson, D.J., Glatzmaier, G.A., and, Schubert, G., 1994, Effects of multiple phase transitions in a 3-D spherical model of convection in the Earths mantle: Journal of Geophysical Research, v. 99, p. 15,877-15,901.

Vacher, P., Mocquet, A., and Sotin, C., 1998, Computation of seismic profiles from mineral physics: the importance of the non-olivine components for explaining the 660 km depth discontinuity: Physics of Earth and Planetary Interiors, v. 106, p. 275-298.

Van den Berg, A.P., Yuen, D.A., and Steinbach, V., 2001, The effects of variable thermal conductivity on mantle heat transfer: Geophysical Research Letters, v. 28, p. 875-878.

Van Keken, P.E., 1997, On entrainment in starting mantle plumes: Earth and Planetary Science Letters, v. 148, p. 1-12.

Von Hertzen, R.P., Cordery, M.J., Dietrick ,R.S., and Fang, C., 1989, Heatflow and thermal origin of hotspot swells: the Hawaiian swell revised: Journal of Geophysical Research, v. 94, p. 13,783-13,799.

Wen, L. and D. L. Anderson, 1997a. Layered mantle convection: A model for geoid and topography and seismology: Earth and Planetary Science Letters, v. 146, p. 367-377.

Wen, L. and D. L. Anderson, 1997b. Slabs, hotspots, cratons and mantle convection revealed

from residual seismic tomography in the upper mantle: Physics of the Earth and Planetary Interiors, v. 99, p. 131-143.

Wessel, P., Smith, W.H.F., 1991 Free software helps map and display data: EOS Transactions of the American Geophysical Union v. 72, p. 441-446.

Wetherill, G.W., 1990, Formation of the Earth: Annual Reviews of Earth and Planetary Science, v.8, p. 205-256.

Whitehead, J.A., and Luther, D.S., 1975, Dynamics of laboratory diapir and plume models: Journal of Geophysical Research, v. 80, p. 705-717.

Wolfe, C.J., Bjarnason, I.Th., Van Decar, J.C. and Solomon, S. C., 1997, Seismic structure of the Iceland mantle plume: Nature, v. 385, p. 245- 247.

Wolfe, C.J., 1998, Prospecting for hotspot roots: Nature, v. 396, p. 212-213.

Zebib, A., Schubert, G., and Straus, J.M., 1980, Infinite Prandtl number thermal convection in a sherical shell: Journal of Fluid Mechanics, v. 97, p. 257.

Zebib, A., Goyal, A.K., and Schubert, G., 1985, Convective motions in a spherical shell: Journal of Fluid Mechanics, v. 152, p. 39-48.

Zhang, S., and Yuen, D.A., 1995, The influence of lower mantle viscosity stratification of 3D spherical-shell mantle convection: Earth and Planetary Science Letters, v. 132, p. 157-166.

Zhong, S., 2006, Constraints on thermochemical convection of the mantle from plume heat flux, plume excess temperature, and upper mantle temperature: Journal of Geophysical Research, v. 111, B04409.

TABLE 1. Parameters used this study along with references. In most cases, these parameters are functions of temperature, pressure and composition. The values shown are global average estimates. Functional forms are discussed in the text.

Parameter	Symbol	Value	Reference
depth	d	2891 km	
gravitational acceleration	g	9.8 m/s^2	
average mantle viscosity	η	$10^{20} - 10^{22}$ Pa s	Mitrovica, 1996
density	ρ	3700-5500 kg m^{-3}	Dziewonski and Anderson, 1982
thermal conductivity	k	3.0 W m^{-1} °K^{-1}	
thermal diffusivity	$\kappa = \frac{k}{\rho c_p}$	$0.9 - 1.2 \times 10^{-6}$ m^2 s^{-1}	
temperature change (non adiabatic)	ΔT	2000°C	Schubert et al., 2001
coefficient of thermal expansion	α	$0.5 - 4.0 \times 10^{-5}$	Chopelas and Boehler, 1992; Chopelas, 2000

TABLE 2. Maximum geoid, topography and heatflow from various grids for a temperature-dependent spherical shell convection calculation.

Grid Name	Grid Size N_θ by N_r	Heat flow Anomaly (mW/m^2)	Topographic Anomaly (m)	Geoid Anomaly (m)
A	50 × 64	21.1	5272.5	151.3
B	75 × 96	18.1	4941.9	145.7
C	100 × 128	17.2	4835.7	144.3
D	125 × 160	16.5	4733.3	142.5
E	150 × 192	16.0	4700.5	142.2
F	175 × 224	15.7	4649.3	141.3

TABLE 3. Results from axisymmetric plume calculations

Rayleigh Number[a]	Internal Heating Rate (W/kg) [b]	Lower Mantle Viscosity Ratio	Coefficient of Thermal Expansion (functional form) [c]	Clapeyron Slope (MPa/K)	Average Temperature	Heatflow Anomaly (mW/m^2)	Topographic Anomaly (m)	Geoid Anomaly (m)
10^6	0.0	1	constant	0.0	0.43	16.0	4700.5	142.1
3×10^6	0.0	1	constant	0.0	0.47	20.7	3770.1	91.9
10^7	0.0	1	constant	0.0	0.51	28.2	3040.7	55.7
3×10^7	0.0	1	constant	0.0	0.55	31.8	2287.9	19.4
10^8	0.0	1	constant	0.0	0.60	43.1	2187.8	11.4
10^6	0.2×10^{-12}	1	constant	0.0	0.46	16.1	4438.5	123.4
10^6	0.4×10^{-12}	1	constant	0.0	0.50	15.9	4185.4	104.9
10^6	0.6×10^{-12}	1	constant	0.0	0.54	15.3	3939.8	85.6
10^6	0.8×10^{-12}	1	constant	0.0	0.66	15.0	4039.0	46.8
10^6	1.0×10^{-12}	1	constant	0.0	0.66	12.9	3745.1	16.4
10^6	0.8×10^{-12}	1	constant	0.0	0.66	15.0	4039.0	46.8
10^6	0.8×10^{-12}	10	constant	0.0	0.55	20.3	4154.9	36.2
10^6	0.8×10^{-12}	30	constant	0.0	0.45	27.9	3380.4	19.4
10^6	0.8×10^{-12}	100	constant	0.0	0.40	33.3	2766.0	6.0
10^6	0.8×10^{-12}	30	constant	0.0	0.45	27.9	3380.4	19.4
10^6	0.8×10^{-12}	30	$(r/ro)^3$	0.0	0.42	27.7	3161.3	48.9
10^6	0.8×10^{-12}	30	$(r/ro)^3$ [d]	0.0	0.51	30.1	2633.9	14.3
10^6	0.8×10^{-12}	30	$(r/ro)^3$	0.0	0.42	27.7	3161.3	48.9
10^6	0.8×10^{-12}	30	$(r/ro)^3$	-1.0	0.42	27.6	3173.3	44.4
10^6	0.8×10^{-12}	30	$(r/ro)^3$	-2.0	0.42	27.4	3187.3	41.7
10^6	0.8×10^{-12}	30	$(r/ro)^3$	-2.8	0.43	27.1	3168.4	28.1
10^6	0.8×10^{-12}	30	$(r/ro)^3$	-2.8	0.33	15.0	2358.1	25.6
10^6	2.4×10^{-12}	30	$(r/ro)^3$	-2.8	0.54	12.9	2130.3	13.4
10^6	4.8×10^{-12}	30	$(r/ro)^3$	-2.8	0.55	12.9	2141.9	12.2

[a] volume averaged
[b] current estimates of mantle heat generation rate are on the order of 7.0×10^{-12} W/kg (Schubert et al., 2001)
[c] volume averaged value of coefficient of thermal expansion used in Rayleigh number
[d] surface value of coefficient of thermal expansion used in Rayleigh number

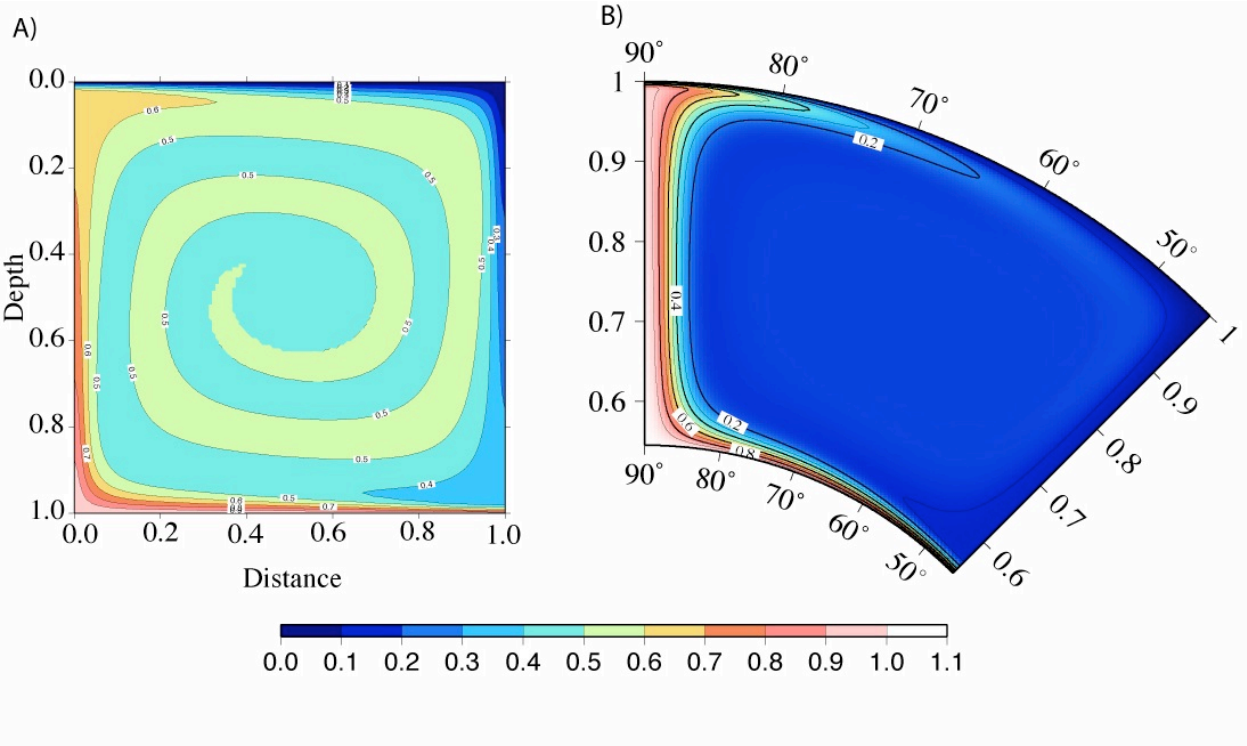

Figure 1. Temperature fields from steady-state constant viscosity, Rayleigh number 10^6 convection calculations in a 1 by 1 Cartesian box (A) and a spherical axisymmetric shell (B) with an inner radius of 0.55 and 45^o co-latitude.

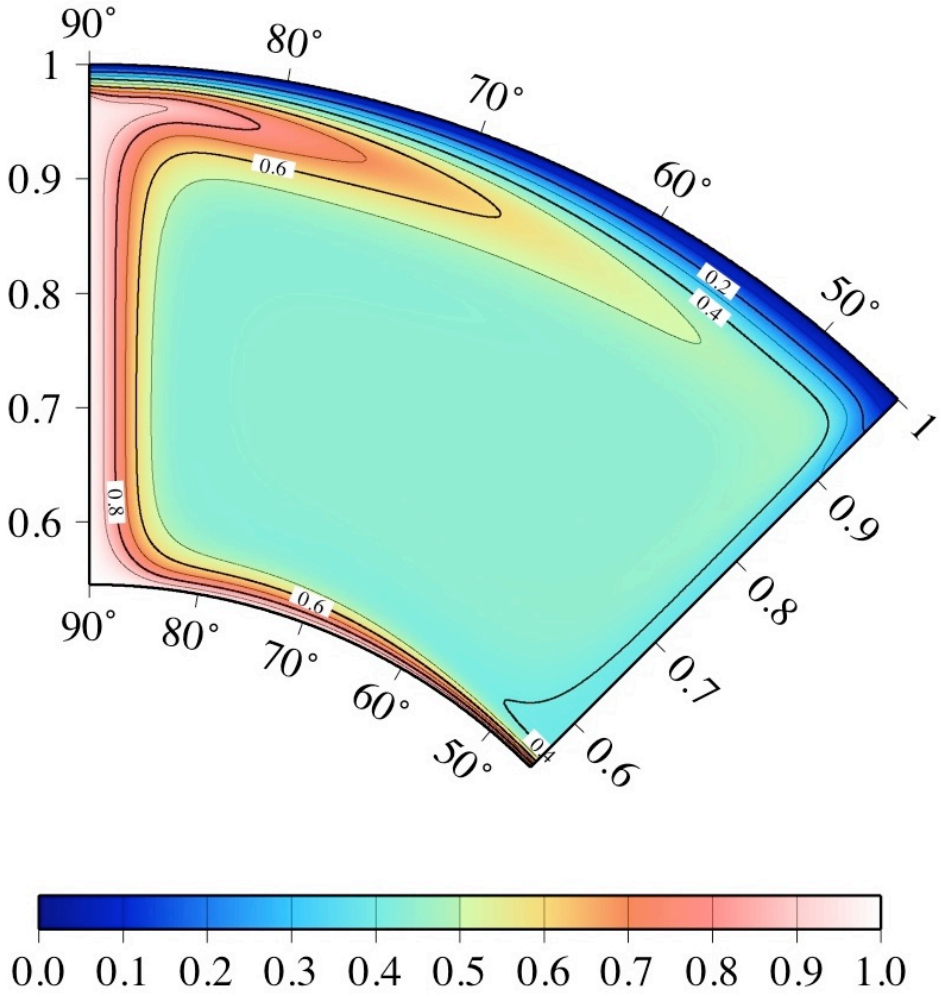

Figure 2. Temperature field from a steady-state temperature-dependent viscosity calculation, with a volume-averaged Rayleigh number 10^6 in a spherical axisymmetric shell with an inner radius of 0.55 and 45^o co-latitude. The activation energy used in the viscosity law is 350 kJ/m^3. The viscosity used in the definition of the Rayleigh number is calculated from the volume-averaged temperature.

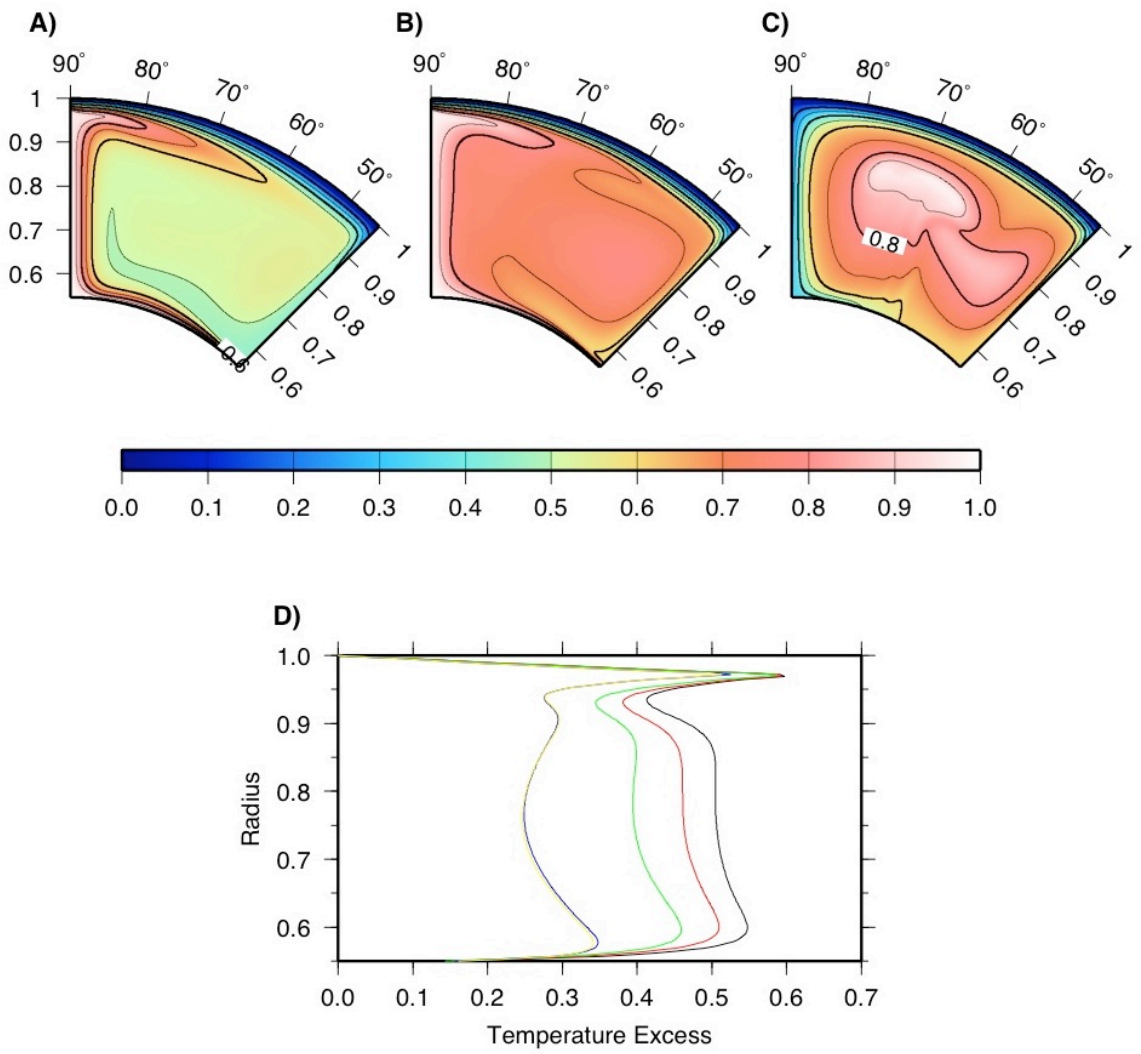

Figure 3. Temperature fields from steady-state temperature-dependent viscosity calculations as in Figure~2 with A) 22% internal heating (0.4x 10^{-12} W/kg internal heating rate), B) 33% internal heating (0.8x 10^{-12} W/kg internal heating rate) and C) 100% internal heating (no bottom heating), D) plot of temperature excess along the center of the plume (i.e., T(theta=0) – Tave) as a function of radius for the calculations with 0.2x 10^{-12} W/kg internal heating rate (black), 0.4x 10^{-12} W/kg internal heating rate (red), 0.6x 10^{-12} W/kg internal heating rate (green), 0.8x 10^{-12} W/kg internal heating rate (blue), and 1.0x 10^{-12} W/kg internal heating rate (yellow).

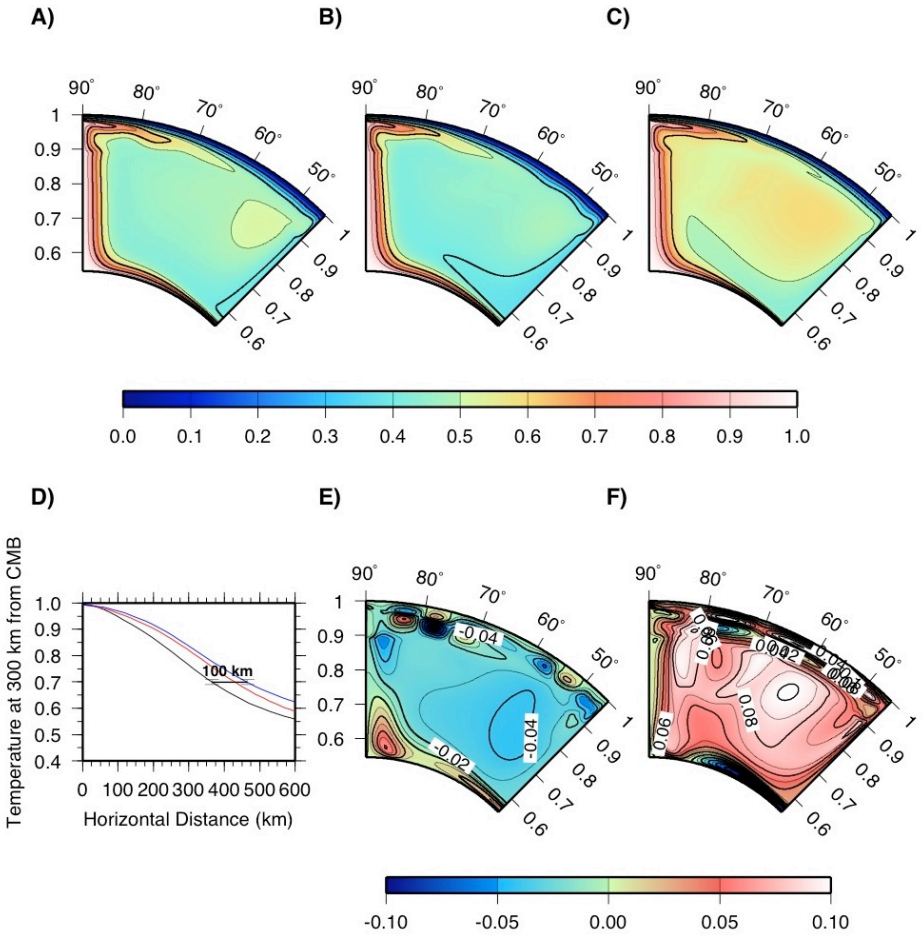

Figure 4. Temperature fields from steady-state temperature-dependent viscosity calculations with 0.8x 10^{-12} W/kg internal heating rate, and a 30-fold increase in viscosity in the lower mantle with A) constant coefficient of thermal expansion with depth, B) coefficient of thermal expansion decreasing like r^3, Rayleigh number based on the surface value of coefficient of thermal expansion C) coefficient of thermal expansion decreasing like r^3 volume-averaged Rayleigh number 10^6, D) plot of temperature at 300 km above the core-mantle boundary as a function of distance from the plume axis for the three cases above (black constant coefficient of thermal expansion, red is volume-averaged, variable coefficient of thermal expansion, blue is variable coefficient of thermal expansion with surface value used for scaling.

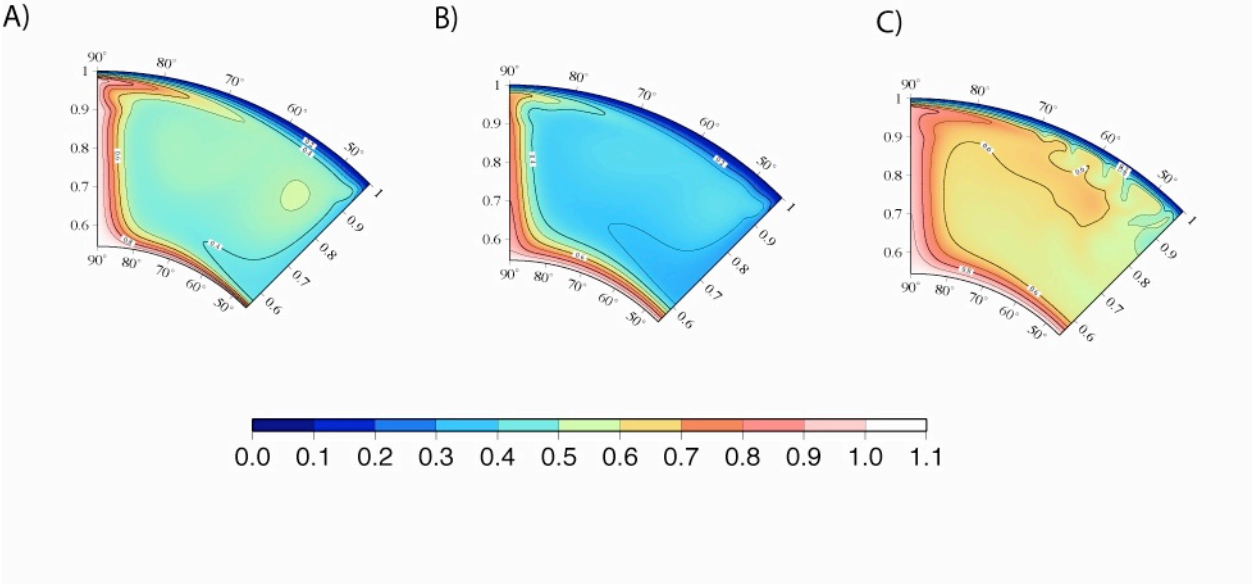

Figure 5. Temperature fields from steady-state temperature-dependent viscosity calculations with 0.8 x 10^{-12} W/kg rate internal heating, and a 30-fold increase in viscosity in the lower mantle, depth-dependent coefficient of thermal expansion, and endothermic phase transformation with A) no basal layer, B) 90~km stably-stratified layer C) 90~km stably-stratified layer and increased rate of internal heating of 4.8 x 10^{-12}W/kg.